Dissipative entanglement generation between two qubits parametrically driven and coupled to a resonator

Sebastián Luciano Gallardo,[1] Daniel Domínguez,[1] and María José Sánchez[1,2]
[1]*Centro Atómico Bariloche and Instituto Balseiro (Universidad Nacional de Cuyo), 8400 San Carlos de Bariloche, Río Negro, Argentina*
[2]*Instituto de Nanociencia y Nanotecnología (INN), CONICET-CNEA, Argentina*

(Received 23 November 2021; revised 14 February 2022; accepted 15 April 2022; published 9 May 2022)

An entangled-state generation protocol for a system of two qubits driven with an ac signal and coupled through a resonator is introduced. We explain the mechanism of entanglement generation in terms of an interplay between unitary Landau-Zener-Stückelberg (LZS) transitions, induced for appropriate frequencies and strong amplitudes of the applied ac signal and dissipative processes dominated by photon loss. In this way, we find that the steady state of the system can be tuned to be arbitrarily close to a Bell state, which is stable against photon loss. Effective two-qubit Hamiltonians that reproduce the resonance patterns associated with LZS transitions are derived.

DOI: 10.1103/PhysRevA.105.052413

I. INTRODUCTION

The generation and stabilization of entangled states is of fundamental importance for quantum information applications. In the last two decades, several proposals explored strategies based on the use of environmental noise to obtain and stabilize steady-state entanglement [1–3].

Most of these schemes used an external driving field as a tool, with examples including adiabatic passage protocols [4] (extensively employed to generate quantum state transfer [5,6]), weak resonant drivings (which enable entanglement stabilization based on tailoring the relaxation rates to generate a highly entangled steady state [7–11]), or a frequency-modulated signal [12] (used to achieve an accelerated formation of dissipative entangled steady states).

These protocols were tested in several systems such as atomic ensembles [13], trapped ions [14–16], Rydberg atoms [5,12], and superconducting qubits [7–11,17], to mention a few.

Recently, a mechanism relying on the amplitude modulation of an ac signal was proposed to generate steady-state entanglement in a system of two coupled qubits driven by a large-amplitude (nonresonant) periodic signal and interacting with a thermal bath [18,19].

Nowadays, circuit quantum electrodynamics (cQED) [20–24] has been established as one of the leading architectures for studying quantum computation and quantum simulation, where superconducting qubits are connected to a transmission line resonator [25–27]. Many important experimental advances have been achieved in this regard, including the observation of the Jaynes-Cummings ladder [28] and long-lived qubit-resonator states [29], entanglement of distant qubits, realization of one- and two-qubit gates, and nondemolition readout operations [11,17,30–37].

In this work we propose a protocol to generate and stabilize maximally entangled states (in particular, Bell states) in a system of two qubits driven with an harmonic signal, which are indirectly coupled via a common resonator. Although this driving protocol was implemented in studies of Landau-Zener-Stückelberg (LZS) interferometry [27,38–42] and entanglement generation [18,19] with superconducting qubits, we are not aware of previous proposals employing ac driven qubits to control entanglement in cQED architectures. Our approach is rather general and not restricted to the usual weak resonant driving, going beyond the standard dispersive regime used to couple the resonator for readout [23]. As is customary in cQED architectures, we will assume that the resonator acts as a filter of noise for the qubits [23,43], protecting them from spontaneous losses to the environment. With this in mind, we will model the environment as a thermal bath coupled to the system mainly through the resonator.

Through an interplay between driving and dissipation, we show that a unique stationary maximally entangled (Bell) state can be obtained, provided the qubits are driven with the appropriate amplitude and frequency. Moreover, the obtained Bell state is protected from environmental effects for as long as the driving is applied.

The paper is organized as follows. In Sec. II we do an overview of the system and present the model Hamiltonian. In Sec. III we solve the unitary driven dynamics of the system and analize the LZS resonance patterns of the two relevant transitions involved in the generation of maximally entangled steady states, once coupling to environment is included in Sec. IV. Additionally, two-qubit Hamiltonians that reproduce the structure of these resonances are also derived in Sec. III. Conclusions and perspectives are given in Sec. V.

II. SYSTEM OVERVIEW

We study a system composed of two qubits coupled to a bosonic mode within a resonator, which is itself weakly coupled to a thermal bath with temperature T_b, as is shown schematically in Fig. 1.

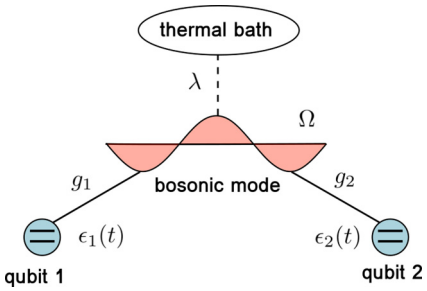

FIG. 1. Schematic representation of the system under study. The qubit $i \in \{1, 2\}$ is periodically driven through $\epsilon_i(t)$ and coupled with strength g_i to a mode of frequency Ω of a resonator. The resonator is weakly coupled to a thermal bath with strength λ via the bosonic operator $a + a^\dagger$.

The Hamiltonian of the qubit $i \in \{1, 2\}$, including the coupling term to the resonator, is given by

$$H_i(t) = \frac{\epsilon_i(t)}{2}\sigma_z^{(i)} + g_i(a + a^\dagger)\sigma_x^{(i)}, \tag{1}$$

where $\sigma_j^{(i)}$ are the Pauli matrices acting on the qubit i and $a^\dagger$ (a) is the creation (destruction) operator of the bosonic mode of the resonator. The qubit i's transition frequency or detuning is ϵ_i, which can be controlled externally as a function of time. The coupling of the qubit i to the resonator is of strength g_i and we suppose that the associated operator is transversal to the qubit i's detuning operator (under this assumption, one can always rotate the qubit basis such that the coupling to the resonator is through $\sigma_x^{(i)}$). A possible qubit i energy gap induced by a term in Eq. (1) transversal to $\sigma_z^{(i)}$ was neglected under the assumption that it is much smaller than the corresponding g_i's, which is rather justified for several superconducting qubit systems [44]. The full Hamiltonian for the cQED architecture is given by

$$H(t) = H_s(t) + H_b + H_{sb}, \tag{2}$$

$$H_s(t) = \Omega a^\dagger a + \sum_{i=1}^{2} H_i(t), \tag{3}$$

where Ω is the resonator mode frequency. The term H_b in Eq. (2) represents the bath Hamiltonian, modeled as a continuum of harmonic oscillators in thermal equilibrium at temperature T_b, with ohmic spectral density $\mathcal{J}(\omega) = \kappa\omega$, where κ is a constant (along this work we take the Boltzmann's constant $k = 1$ and also $\hbar = 1$). The term H_{sb} stands for the interaction between the system and the thermal bath, which in this work we suppose is through the operator $(a + a^\dagger)$ and of strength λ. The explicit forms of H_b and H_{sb} are given in Appendix A.

The driving required for the Bell-state generation protocol depends on the relative sign of the couplings g_i. We suppose that the couplings are similar in magnitude, but their relative sign could be either equal or opposite, corresponding to couplings to even or odd modes of the resonator, respectively. In the following without loss of generality we will consider couplings with the same sign and the drivings in detuning chosen as

$$\epsilon(t) \equiv \epsilon_1(t) = \epsilon_2(t) = A\cos(\omega t), \tag{4}$$

with A the amplitude and ω the frequency of the driving. For the case of opposite coupling signs, the driving should be chosen to be $\epsilon_1(t) = -\epsilon_2(t)$. It can be shown that both cases are related by a local unitary transformation $H \to \sigma_y^{(2)} H \sigma_y^{(2)}$, which keeps the entanglement generation dynamics invariant.

As we will discuss in detail in Sec. IV, to stimulate the LZS resonances necessary for this Bell-state generation protocol we require that $0 < |\delta_g| \ll g_1 g_2/\Omega$, with $\delta_g \equiv g_1 - g_2$. As the relevant involved transitions occur in a timescale δ_g^{-1}, the smaller δ_g, the longer it will take to reach the stationary Bell state.

To solve numerically the dynamics in the purely unitary case [considering only $H_s(t)$ in Eq. (2)], we diagonalize the evolution operator over a period of the driving using a fourth-order Trotter-Suzuki expansion. In this way we obtain the Floquet states and the associated quasienergies [45]. To study the open dynamics, we evolved the system's density operator using the Floquet-Born-Markov (FBM) master equation [41,46,47] within a moderate rotating wave approximation (RWA), as is detailed in Appendix B. For the numerical simulations we truncate the Hilbert space to a finite number of photon levels. We found that retaining the first five photon levels was sufficient to attain convergence.

III. UNITARY DYNAMICS

In this section we focus on the unitary dynamics described by the Hamiltonian $H_s(t)$ defined in Eq. (3). As the system is driven through $\epsilon(t)$ it is relevant to study the energy spectrum of H_s parametrized as a function of ϵ, shown in Fig. 2.

For the following analysis, it will be useful to define the set of Bell states of the two-qubit system: $|\Phi_\pm\rangle \equiv \frac{1}{\sqrt{2}}(|\uparrow\uparrow\rangle \pm |\downarrow\downarrow\rangle)$ and $|\Psi_\pm\rangle \equiv \frac{1}{\sqrt{2}}(|\uparrow\downarrow\rangle \pm |\downarrow\uparrow\rangle)$, where $\sigma_z|\uparrow\rangle = |\uparrow\rangle$, and $\sigma_z|\downarrow\rangle = -|\downarrow\rangle$. The Bell states are maximally entangled and form a basis for the two-qubit Hilbert space.

The structure of the spectrum of Fig. 2 away from all avoided crossings (AC) is rather simple, the energies and eigenstates satisfy

$$H_s(\epsilon)\,|N\uparrow\uparrow\rangle \approx (N\Omega + \epsilon)\,|N\uparrow\uparrow\rangle, \tag{5}$$

$$H_s(\epsilon)\,|N\Psi_\pm\rangle \approx N\Omega\,|N\Psi_\pm\rangle, \tag{6}$$

$$H_s(\epsilon)\,|N\downarrow\downarrow\rangle \approx (N\Omega - \epsilon)\,|N\downarrow\downarrow\rangle, \tag{7}$$

with $|N\rangle$ the state of the resonator with N photons.

The aim is to identify the AC that are reached by the amplitude A of the driving since, in this case, the nonperturbative LZS mechanism [38,39,44,48] is triggered. The relevant avoided crossings (AC) are shown in Fig. 2 and labeled by an integer number N and a $\pm$ sign to identify an AC located at $\epsilon = \pm\Omega$, respectively. The $N\pm$ AC involves the four states $|(N \mp 1)\uparrow\uparrow\rangle$, $|N\Psi_+\rangle$, $|N\Psi_-\rangle$, and $|(N \pm 1)\downarrow\downarrow\rangle$. In this AC the levels $|(N \mp 1)\uparrow\uparrow\rangle$, $|N\Psi_+\rangle$, and $|(N \pm 1)\downarrow\downarrow\rangle$ are mixed with each other by an energy of the order of $\sqrt{N+1}g_i$, while the $|N\Psi_-\rangle$ is mixed with a superposition of $|(N \mp 1)\uparrow\uparrow\rangle$ and $|(N \pm 1)\downarrow\downarrow\rangle$ by an energy of the order of $\sqrt{N+1}\delta_g$, giving

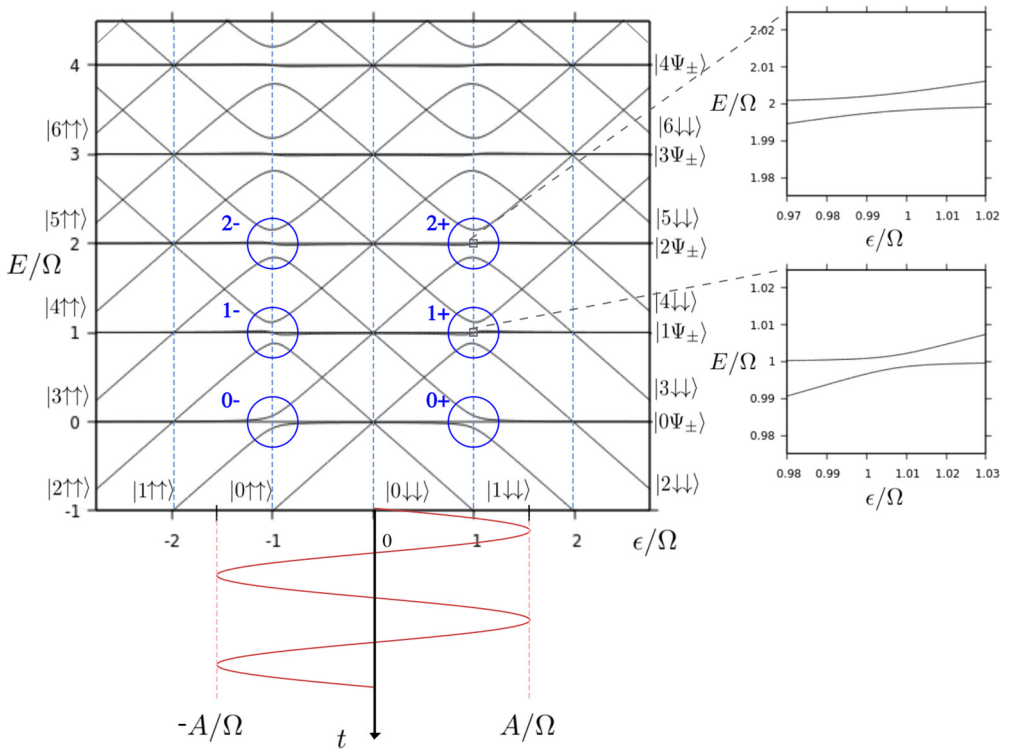

FIG. 2. Energy spectrum of H_s [Eq. (3)] parametrized a function of ϵ/Ω, for $g_1 = 0.05\Omega$ and $g_2 = 0.0485\Omega$. AC are located at integer and half-integer values of ϵ/Ω. Those at $\epsilon = \pm\Omega$, labeled as $N\pm$ are of first order in g_i and δ_g while all others are of second and higher order in g_i and δ_g. A zoomed-in view of 1+ and 2+ AC is shown, such that the gap of order δ_g can be seen. The system is driven by a harmonic driving $\epsilon(t) = A\cos(\omega t)$. Integer values of ϵ/Ω are marked with dotted lines. The asymptotic eigenstates away from AC are shown. See text for more details.

rise to smaller gaps, examples of which can be seen in the blown up right panel of Fig. 2 for the 1+ and 2+ AC (see Appendix C for analytic details on the derivation of these mixing strengths).

The other AC in the energy spectrum are of quadratic or higher order in g_i and δ_g and are not relevant for the LZS transitions studied in this paper.

It can be readily seen from Eq. (3) that for $g_1 = g_2$ ($\delta_g = 0$), the singlet states $|N\Psi_-\rangle$ are exact eigenstates of $H_s(\epsilon)$ with energy $N\Omega$. Since they are also eigenstates of the driving operator [$\propto (\sigma_z^{(1)} + \sigma_z^{(2)})$], transitions involving the states $|N\Psi_-\rangle$ are forbidden for $\delta_g = 0$. However, when $\delta_g \neq 0$, LZS transitions involving these levels become possible.

In what follows we consider explicitly the LZS interferometry for transitions involving the $|0\Psi_-\rangle$ and $|1\Psi_-\rangle$ states and the passage through the $N\pm$ AC by means of the harmonic driving of $\epsilon(t)$. These transitions will be relevant for the Bell-state generation mechanism once dissipation is included.

A. Transitions to $|1\Psi_-\rangle$

We begin by studying the transition probability for $|0\uparrow\uparrow\rangle \to |1\Psi_-\rangle$ induced by the periodic driving. We are interested in this transition because, as we will discuss in Sec. IV, $|1\Psi_-\rangle$ will decay into $|0\Psi_-\rangle$ after including dissipation, which is a maximally entangled state that is stable against photon loss.

We recall that in two-level LZS interferometry, when a quantum system is driven through an AC of magnitude $\tilde{\Delta}$ by an harmonic signal of amplitude A and frequency ω, the n-resonance condition in the fast driving regime (i.e., $A\omega \gg \tilde{\Delta}^2$) is $\Delta\bar{E} = n\omega$, where $\Delta\bar{E}$ is the average energy difference between the two involved states over a period of the driving [27,38,49–52]. At the resonance condition the transfer of population between both states involved in the AC is maximum. However, as the LZS resonance patterns have a width $\propto \tilde{\Delta}\, J_n(A/\omega)$, with J_n the nth Bessel function [48], at the zeros of J_n the transition probability vanishes giving rise to a phenomenon known as coherent destruction of tunneling [53].

In the present case and considering only the two levels $|0\uparrow\uparrow\rangle$ and $|1\Psi_-\rangle$, the average energy difference is given by Ω (due to the symmetric driving this is the energy difference at $\epsilon = 0$) while the magnitude of the gap at the 1+ AC between these two states is proportional to δ_g, as we already discussed. Therefore, LZS resonance patterns centered around $\Omega/\omega = n$ and of width $\propto \delta_g J_n(A/\omega)$ [48] are expected for the transition $|0\uparrow\uparrow\rangle \to |1\Psi_-\rangle$ and indeed are observed, as is shown in Fig. 3.

In Fig. 4(a) the detailed structure of the LZS interferometry pattern associated to the resonance $\Omega/\omega = 2$ as a function of Ω/ω and A/ω is shown. A modulation of the resonance with $J_2(A/\omega)$ is also observed as a function of A/ω, consistently with the aforementioned description (a similar behavior is obtained for other resonances at integer values of n). However, the curvature of the resonance observed as a function of A/ω is not captured under the assumption of describing this transition solely as a two-level transition. We numerically find that the curvature is an effect of order $g_1 g_2/\Omega$, as we plot in Fig. 5(a),

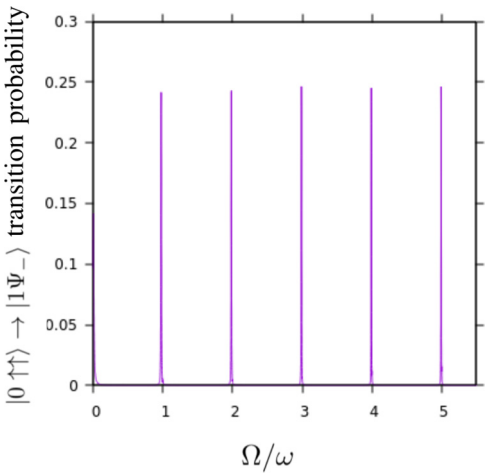

FIG. 3. Unitary time-averaged transition probabilities calculated numerically for the transition $|0\uparrow\uparrow\rangle \to |1\Psi_-\rangle$. Resonances are seen for integer values of Ω/ω. The qubit-resonator coupling strengths used are $g_1 = 0.1\omega$ and $g_2 = 0.097\omega$ and the amplitude of the driving is $A = \Omega$.

where the transition probability as a function of Ω/ω and g/ω with $g \equiv (g_1 - g_2)/2$ is shown.

In what follows we will derive an effective two-qubit Hamiltonian from which the structure of the resonances for the $|0\uparrow\uparrow\rangle \to |1\Psi_-\rangle$ transition, including their curvature as a function of A/ω, can be obtained.

As was explained earlier in this section, the initial state $|0\uparrow\uparrow\rangle$ is strongly mixed with the states $|1\Psi_+\rangle$ and $|2\downarrow\downarrow\rangle$ at the $2+$ AC. However, the transition from $|0\uparrow\uparrow\rangle$ to $|1\Psi_+\rangle$ is considerably favored over the transition from $|0\uparrow\uparrow\rangle$ to $|2\downarrow\downarrow\rangle$ (as explained at the end of Appendix C), such that we can neglect the population transfer to the later state. Under this approximation, the $|0\uparrow\uparrow\rangle$ state will transition mostly to $|1\Psi_+\rangle$ state and in a lesser degree, via the AC of order δ_g, to $|1\Psi_-\rangle$. In addition, the $|1\Psi_+\rangle$ state will be strongly mixed with the $|0\downarrow\downarrow\rangle$ state in the $2-$ AC.

Therefore, from the previous argument, we expect that, for the transition $|0\uparrow\uparrow\rangle \to |1\Psi_-\rangle$, the most populated states will be in the subspace S_1 spanned by $\{|0\uparrow\uparrow\rangle, |0\downarrow\downarrow\rangle, |1\Psi_\pm\rangle\}$. Projecting the Hamiltonian Eq. (3) into S_1, the state of the resonator becomes uniquely determined by the state of the qubits (within S_1). Thus one can write the terms involving resonator operators in Eq. (3) in terms of qubit operators

$$\begin{aligned} a^\dagger a|_{S_1} &= |1\Psi_+\rangle\langle 1\Psi_+| + |1\Psi_-\rangle\langle 1\Psi_-| \\ &= \tfrac{1}{2}\big(1 - \sigma_z^{(1)}\sigma_z^{(2)}\big), \end{aligned} \tag{8}$$

and

$$\begin{aligned} \tfrac{1}{2}(a + a^\dagger)\big(\sigma_x^{(1)} \pm \sigma_x^{(2)}\big)|_{S_1} &= |0\Phi_\mp\rangle\langle 1\Psi_\pm| + |1\Psi_\pm\rangle\langle 0\Phi_\mp| \\ &= \tfrac{1}{2}\big(\sigma_x^{(1)} \pm \sigma_x^{(2)}\big), \end{aligned} \tag{9}$$

where now $\sigma_j^{(i)}$ are understood as 4×4 matrices and $|_{S_1}$ indicates projection into S_1. Replacing the above expressions into Eq. (3), one arrives at the effective time-dependent Hamiltonian, valid for studying the transition $|0\uparrow\uparrow\rangle \to |1\Psi_-\rangle$:

$$H_I(t) = \sum_i \Big(\frac{\epsilon(t)}{2}\sigma_z^{(i)} + g_i\sigma_x^{(i)}\Big) - \frac{\Omega}{2}\sigma_z^{(1)}\sigma_z^{(2)} + \frac{\Omega}{2}. \tag{10}$$

Notice that Eq. (10) is the Hamiltonian of two driven qubits coupled longitudinally studied in Ref. [54]. In the present case, Ω plays the role of the interaction strength between the qubits and $2g_i$ the role of the intrinsic qubit gaps.

In Fig. 4(b) the time-averaged transition probability $|0\uparrow\uparrow\rangle \to |1\Psi_-\rangle$ computed numerically using Eq. (10) is displayed. The agreement with Fig. 4(a), obtained from the full Hamiltonian Eq. (3), is excellent, thus confirming the assumptions that led to the effective Hamiltonian of Eq. (10).

B. Transitions out of $|0\Psi_-\rangle$

We now shift our attention to the time-averaged probabilities for the $|0\Psi_-\rangle \to$ (other states) transition, which is defined as the sum of all transition probabilities from the initial state $|0\Psi_-\rangle$ to any other states orthogonal to it. We are interested in this transition because it is an indicator of the stability of $|0\Psi_-\rangle$ against unitary transitions induced by the driving that might take the system out of this state. Figure 4(c) shows numerical results for the corresponding transition probabilities using the full Hamiltonian Eq. (3).

The LZS resonance condition for both transitions, $|0\Psi_-\rangle \to |1\uparrow\uparrow\rangle$ and $|0\Psi_-\rangle \to |1\downarrow\downarrow\rangle$, is again $\Omega/\omega = n$ for some integer n. Resonances around these values of Ω/ω of width $\propto \delta_g J_n(A/\omega)$ are expected and observed in Fig. 4(d), in analogy to the results of Sec. III A. The effect of g on the curvature of the resonances out of $|0\Psi_-\rangle$ is again of order $g_1 g_2/\Omega$, but of opposite sign to that of the transitions to $|1\Psi_-\rangle$, as can be seen in Fig. 5(b). This implies that there are values of the driving parameters, A and ω, for which the transitions to $|1\Psi_-\rangle$ are stimulated but those out of $|0\Psi_-\rangle$ are not. This is the key point that will be made use of to generate Bell states once dissipation is included, as is explained in the next section.

We will now derive another effective two-qubit Hamiltonian for studying the $|0\Psi_-\rangle \to$ (other states) transition. The initial state $|0\Psi_-\rangle$ is mixed with the $|1\uparrow\uparrow\rangle$ and $|1\downarrow\downarrow\rangle$ states in the $1-$ and $1+$ AC, respectively. Again neglecting transitions between $|(N\mp 1)\uparrow\uparrow\rangle$ and $|(N\pm 1)\downarrow\downarrow\rangle$ in the $N\pm$ AC (see Appendix C), the population in these two states will transition to $|0\Psi_+\rangle$ in the $1\pm$ AC and to $|2\Psi_+\rangle$ in the $3\pm$ AC.

Thus in the present case, and unlike the analysis of Sec. III A, five linearly independent states are, in principle, involved in the transition under study. However, since the $3\pm$ crossings that populate $|2\Psi_+\rangle$ involve a greater mixing between states than the $1\pm$ crossings, that populate $|0\Psi_+\rangle$ (because the gap magnitude increases with N, as can be seen in Fig. 2 and is shown in Appendix C), we neglect the population transferred to $|0\Psi_+\rangle$. Therefore, under these approximations, we expect that the most populated states will be in the subspace S_2 spanned by $\{|0\Psi_\pm\rangle, |1\uparrow\uparrow\rangle, |1\downarrow\downarrow\rangle, |2\Psi_+\rangle\}$. Projecting the operators of the Hamiltonian Eq. (3) into S_2, one obtains

$$\begin{aligned} a^\dagger a|_{S_2} &\approx |1\Phi_+\rangle\langle 1\Phi_+| + |1\Phi_-\rangle\langle 1\Phi_-| + 2\,|2\Psi_+\rangle\langle 2\Psi_+| \\ &= 1 + \tfrac{1}{2}\big(\sigma_x^{(1)}\sigma_x^{(2)} + \sigma_y^{(1)}\sigma_y^{(2)}\big), \end{aligned} \tag{11}$$

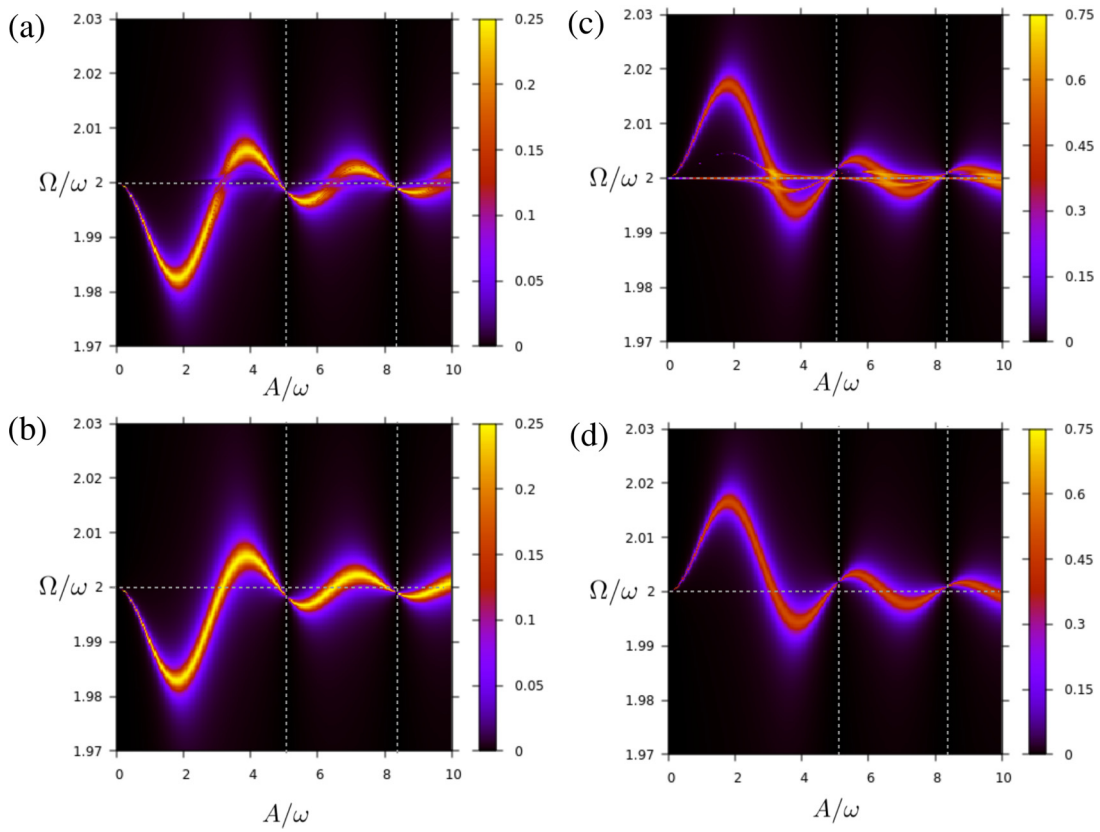

FIG. 4. Upper panel: Unitary time-averaged transition probabilities calculated numerically with the Hamiltonian Eq. (3) for the transitions (a) $|0\uparrow\uparrow\rangle \to |1\Psi_-\rangle$ and (c) $|0\Psi_-\rangle \to$ (other states), as a function of A/ω and Ω/ω. The patterns show resonances at $\Omega/\omega = n \in \mathbb{N}$ with width of order δ_g modulated by the nth Bessel function $J_n(A/\omega)$. Lower panel: Transition probabilities for (b) $|0\uparrow\uparrow\rangle \to |1\Psi_-\rangle$ and (d) $|0\Psi_-\rangle \to$ (other states), calculated using the effective two-qubit Hamiltonians Eqs. (10) and (13), respectively. The line $\Omega/\omega = 2$ and the lines for which A/ω equals the first two zeros of the second Bessel function are indicated with gray dotted lines. In all cases the qubit-resonator coupling strengths used are $g_1 = 0.1\omega$ and $g_2 = 0.097\omega$.

$$\tfrac{1}{2}(a+a^\dagger)\big(\sigma_x^{(1)} \pm \sigma_x^{(2)}\big)|_{S_2} \approx |0\Psi_\pm\rangle\langle 1\Phi_\mp| + |1\Phi_\mp\rangle\langle 0\Psi_\pm| = \tfrac{1}{2}\big(\sigma_x^{(1)} \pm \sigma_x^{(2)}\big), \tag{12}$$

and we arrive at the effective Hamiltonian, valid for studying the transition $|0\Psi_-\rangle \to$(other states)

$$H_{\rm tr}(t) = \sum_i \left(\frac{\epsilon(t)}{2}\sigma_z^{(i)} + g_i\sigma_x^{(i)}\right) + \frac{\Omega}{2}\big(\sigma_x^{(1)}\sigma_x^{(2)} + \sigma_y^{(1)}\sigma_y^{(2)}\big) + \Omega, \tag{13}$$

which is the Hamiltonian of two transversally coupled and symmetrically driven qubits, with Ω playing the role of the interaction strength and $2g_i$ the role of the intrinsic qubit gaps [54].

Numerical results for the transition probability $|0\Psi_-\rangle \to$ (other states) computed from Eq. (13) are shown in Fig. 4(d). Except for the additional thinner resonances around integer Ω/ω, which correspond to resonances to states outside S_2, the agreement with Fig. 4(c), obtained using the full Hamiltonian Eq. (3) is remarkable.

IV. DISSIPATION-INDUCED BELL-STATE GENERATION

In the previous section we concluded that, starting from the initial state $|0\uparrow\uparrow\rangle$, there are regions in the $A/\omega - \Omega/\omega$ plane where a unitary resonance to $|1\Psi_-\rangle$ is stimulated but no unitary resonance involving $|0\Psi_-\rangle$ is so. When the driving amplitude A and frequency ω are chosen as to select one of these points, the process

$$|0\uparrow\uparrow\rangle \overset{H_s(t)}{\to} |1\Psi_-\rangle \overset{\rm PL}{\to} |0\Psi_-\rangle \tag{14}$$

can occur once dissipation is included, where the first transition is unitary and induced by the driven Hamiltonian $H_s(t)$, and the second one is the loss of a photon to the environment. The same process can also take place when starting from $|0\downarrow\downarrow\rangle$ or $|0\Psi_+\rangle$ since they show similar unitary resonances for $|0\downarrow\downarrow\rangle \to |1\Psi_-\rangle$ and $|0\Psi_+\rangle \to |1\Psi_-\rangle$.

Since the open system dynamics is linear due to the weak coupling to the environment (see Appendix B for details), one can understand the evolution of the system's density matrix as the independent evolution of its ensemble members which, for $T_{\rm b} \ll \Omega$, will eventually reach one of the states with zero photons. If the reached states are different from $|0\Psi_-\rangle$, they will go through the process defined in Eq. (14) ending up at least partially in $|0\Psi_-\rangle$. As all transitions involving $|0\Psi_-\rangle$

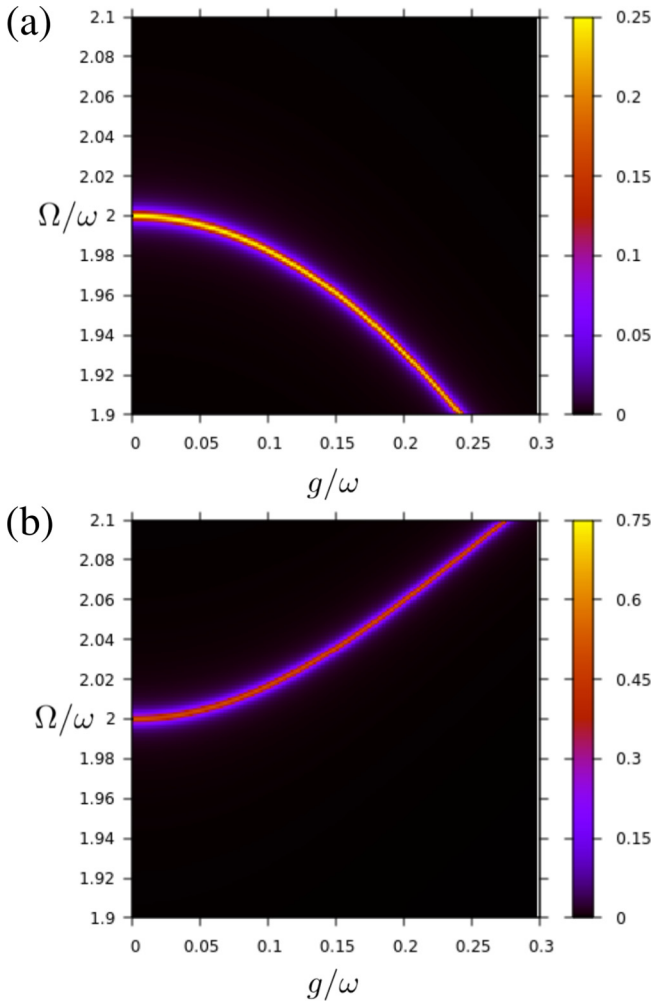

FIG. 5. Unitary time-averaged transition probabilities for the transitions (a) $|0\uparrow\uparrow\rangle \to |1\Psi_-\rangle$ and (b) $|0\Psi_-\rangle \to$(other states) calculated using the effective Hamiltonians Eqs. (10) and (13), respectively, as a function of g/ω and Ω/ω, for $\delta_g = 0.003\omega$ and $A = \Omega$. For small g, an approximately quadratic dependence of the resonance displacement as a function of g is observed, with opposite curvature for both transitions.

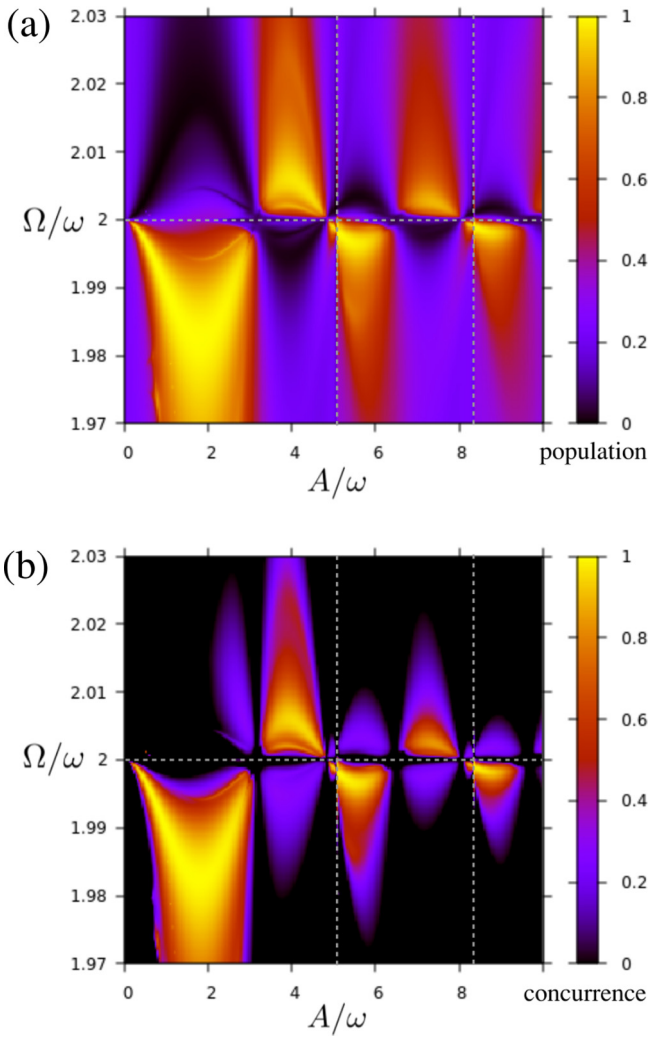

FIG. 6. Time-averaged (a) population of $|0\Psi_-\rangle$ and (b) concurrence of the steady state of the driven dissipative system of two qubits coupled to a resonator, obtained after solving numerically the FBM master equation associated to the Hamiltonian defined in Eq. (2). Asymmetrical resonances are observed at integer values of Ω/ω. The coupling strengths are the same as in Fig. 4, with bath parameters $\kappa\lambda^2 = 0.0001$ and $T_b = 0.001\omega$. The line $\Omega/\omega = 2$ and the lines for which A/ω equals the first two zeros of the second Bessel function are indicated with gray dotted lines.

are out of resonance, gradually the population of the system's density matrix accumulates in this state.

Figure 6(a) shows numerical results for the time averaged population of $|0\Psi_-\rangle$ in the stationary state as a function of A/ω and Ω/ω obtained after solving numerically the FBM master equation for the system's density matrix ρ (see Appendix B for details).

The stationary state is found to be unique and T periodic in time. The behavior of the stationary population closely follows what is predicted by the previous argument: population maxima very close to 1 are observed for points in the parameter space along the unitary resonance patterns of $|0\uparrow\uparrow\rangle \to |1\Psi_-\rangle$ and population minima, very close to 0, are obtained for points along the unitary $|0\Psi_-\rangle \to$ (other states) resonances.

To quantify the degree of entanglement of the qubits, we use the concurrence as a measure [55],

$$\mathcal{C}[\rho_q] = \max\{0, r_3 - r_2 - r_1 - r_0\}, \tag{15}$$

defined in terms of the qubits' density matrix $\rho_q = \mathrm{Tr}_r(\rho)$, where the trace operation is over the states of the resonator and r_i are the real-valued eigenvalues of

$$\sqrt{\sqrt{\rho_q}\sigma_y^{(1)}\sigma_y^{(2)}\rho_q^*\sigma_y^{(1)}\sigma_y^{(2)}\sqrt{\rho_q}}, \tag{16}$$

sorted in ascending order, where ρ_q^* is the complex conjugate of ρ_q and the conjugation must be done in a separable basis. The concurrence takes a value of 0 for a separable state, a value of 1 for a maximally entangled state, and values in between for partially entangled states.

Figure 6(b) shows the time-averaged concurrence of the stationary state. It is observed that the maxima of the concurrence that are close to 1 are achieved only when the state $|0\Psi_-\rangle$ is populated, indicating that this is the only maximally

entangled state that is generated. It is also noteworthy that, for driving parameters lying outside the mentioned resonances, which constitute the vast majority of the points in the $A/\omega - \Omega/\omega$ plane (including the case of no driving at all $A = 0$), the stationary state is either separable or almost separable.

As we already mentioned, to attain $|0\Psi_-\rangle\langle 0\Psi_-|$ as the stationary state of the system, a necessary condition is to find points in the plane $A/\omega - \Omega/\omega$ where the resonance conditions for the transitions to $|1\Psi_-\rangle$ and out of $|0\Psi_-\rangle$ do not overlap. This can only be fulfilled if the maximum resonance deviation from the condition $\Omega/\omega = n$ (of order $g_1 g_2/\Omega$) is much greater than the resonance width (of order δ_g), and this the source of the requirement $\delta_g \ll g_1 g_2/\Omega$. The optimal entanglement generation (maximal area and intensity of concurrence patterns) is achieved for amplitudes $A \approx \Omega$ and frequencies ω such that Ω is below an integer multiple of ω by a frequency of the order of $g_1 g_2/\Omega$, i.e. $A = \Omega = n\omega - \mathcal{O}(g_1 g_2/\Omega)$.

Finally, Fig. 7 shows the temporal dynamics of relevant populations of the system's density matrix at a point of high entanglement generation $A = \Omega = 1.983\omega$, for the system starting in the state $\rho_0 = |0\uparrow\uparrow\rangle\langle 0\uparrow\uparrow|$. It is seen that, even though the dynamics of the populations is complicated, a clear resonance to the state $|0\Psi_+\rangle$ is stimulated in a timescale of the order of δ_g^{-1}, which gradually decays into $|0\Psi_-\rangle$ via photon loss to the environment. Population accumulates in this state, and given enough time the system ends up essentially at $\rho_\infty = |0\Psi_-\rangle\langle 0\Psi_-|$. Notice that the fast temporal oscillations observed in the populations of the $|0\uparrow\uparrow\rangle$ and $|0\uparrow\uparrow\rangle$ states are related to the effective Rabi frequency for the transitions between the involved states, which, as we already stressed, is proportional to $gJ_2(A/\omega)$ (for this analysis we take $g_1 = g_2 = g$ without loss of generality). Being $g \sim 0.1\omega$, the period of the fast oscillations results $\propto 1/g \sim 10T$. As the scale of the temporal axis goes to 1000 T hundreds of oscillations are observed. On the other hand, the entangled state $|0\Psi_+\rangle$ is stimulated in a timescale of order $\delta_g^{-1} \sim 330T$, as can be observed in Fig. 7.

We thus conclude that by applying a driving with appropriate amplitude and frequency it is possible to populate the maximally entangled state $|0\Psi_-\rangle$ independently of the initial state of the system.

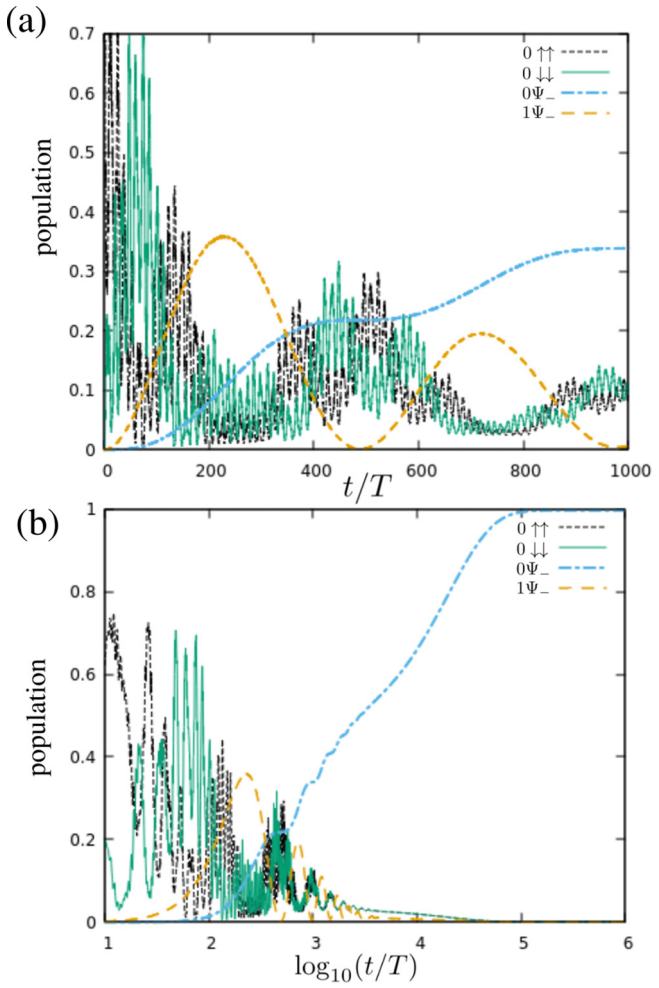

FIG. 7. Temporal dependence of the system's density matrix populations, starting from the initial state $|0\uparrow\uparrow\rangle\langle 0\uparrow\uparrow|$, for up to (a) 1000 (linear scale) and (b) 10^6 (log scale) driving periods, dissipation included. The driving parameters are $A = \Omega = 1.983\omega$ and the rest of the parameters are the same as in Fig. 6. The populations of $|0\uparrow\uparrow\rangle$, $|0\downarrow\downarrow\rangle$, $|0\Psi_-\rangle$, and $|1\Psi_-\rangle$ are shown. It is seen that for short times a resonance between $|0\uparrow\uparrow\rangle$, $|0\downarrow\downarrow\rangle$, and $|1\Psi_-\rangle$ is stimulated. For later times and via photon loss population gradually accumulates in $|0\Psi_-\rangle$.

V. CONCLUSION

In this work we presented an entanglement generation protocol for a system of two qubits coupled through a resonator. A maximally entangled steady state is achieved when a symmetric ac driving, with appropriate frequency and large amplitudes, is applied over both qubits. The optimal steady-state entanglement generation is attained for driving amplitudes $A \approx \Omega$ and frequencies such that Ω/ω is slightly below an integer number.

The areas of entanglement generation in the A/ω-Ω/ω plane are associated to resonant unitary transitions into $|1\Psi_-\rangle$ and out of $|0\Psi_-\rangle$. If the driving is such that transitions to $|1\Psi_-\rangle$ are in resonance, but transitions out of $|0\Psi_-\rangle$ are not, once dissipation is included the system will accumulate population in $|0\Psi_-\rangle$ via photon loss from $|1\Psi_-\rangle$. All the relevant features of the unitary resonance patterns were described in terms of effective Hamiltonians for two driven qubits. This, in addition to drastically reducing the original dimension of the Hilbert space, allows the straightforward analysis of the resonance patterns, as the LZS interferometry for the two-qubit systems described by the effective Hamiltonians, Eqs. (10) and (13), was already studied in Refs. [19,54].

The main advantage of the proposed protocol is that it enables the generation of steady-state entanglement for a broader range of frequencies and amplitudes, compared to the traditional schemes for entanglement generation that make use of weak and resonant driving.

The fact that, due to dissipation, the steady state is independent of the initial state of the system [1,2], guarantees that the obtained entangled state is protected from environmental effects for as long as the driving is applied.

Moreover, the present proposal allows entangling distant and strongly driven qubits which are, for example, a

microwave waveguide apart. Therefore, it is expected that our scheme could add a robust means to realize entanglement protocols in setups extensively used nowadays in cQED [23,24].

ACKNOWLEDGMENTS

We acknowledge support from CNEA, CONICET (PIP11220150100756), ANPCyT (PICT2016-0791 and PICT2019-0654), and UNCuyo (06/C591). We thank Leandro Tossi for comments and conversations on this manuscript.

APPENDIX A: MODEL OF THE ENVIRONMENT

We model the bath and its interaction with the system using the Caldeira-Leggett model [56]

$$H_{\mathrm{b}} = \int_0^\infty d\omega \omega b_\omega^\dagger b_\omega, \tag{A1}$$

$$H_{\mathrm{sb}} = \lambda A \int_0^\infty d\omega \sqrt{\mathcal{J}(\omega)}(b_\omega + b_\omega^\dagger) + H_{\mathrm{rn}}, \tag{A2}$$

$$H_{\mathrm{rn}} = \lambda^2 A^2 \int_0^\infty d\omega \frac{\mathcal{J}(\omega)}{\omega}, \tag{A3}$$

where b_ω and $b_\omega^\dagger$ are the creation and destruction operators of the harmonic oscillator continuum, A is a unitless system operator, λ is a coupling strength, and H_{rn} is a renormalization term to cancel all Lamb shifts induced on the system by the thermal bath.

For the system under study we chose $A = a + a^\dagger$ and $\mathcal{J}(\omega) = \kappa\omega$, with κ a constant with units of energy^{-2}. Usually, it is necessary to put a cutoff frequency in the bath spectral density, but for our purposes, and since we already canceled out the Lamb shifts, it is permissible to take this cutoff frequency as infinity (greater than all energy scales of the problem) as we have implicitly done by the choice of $\mathcal{J}(\omega)$.

APPENDIX B: FLOQUET-BORN-MARKOV MASTER EQUATION

Floquet theory is widely used to study time periodic unitary quantum systems [45]. It shows that for a quantum system with a T-periodic Hamiltonian $H(t)$, all solutions are a linear combination of a single basis of states of the form $e^{-i\epsilon_\alpha t}\,|u_\alpha(t)\rangle$. Here, $|u_\alpha(t)\rangle$ is T periodic and is called a Floquet state and ϵ_α is called its corresponding quasienergy. To find the Floquet states and their quasienergies it is customary to diagonalize the evolution operator $U(t, t_0)$ over a period of the driving since the Floquet states satisfy the eigenvalue equation

$$U(t+T, t)\,|u_\alpha(t)\rangle = e^{-i\epsilon_\alpha T}\,|u_\alpha(t)\rangle\,. \tag{B1}$$

The Floquet-Born-Markov master equation allows modeling dissipative processes in periodically driven systems [40,46,47,57,58]. Assuming a sufficiently weak coupling to the environment, such that the thermal bath autocorrelation time $\tau_c = h/kT_b$ is much smaller than the timescale for relaxation [57,58], a linear Markovian differential equation for the time evolution of the system's density matrix is obtained:

$$\partial_t \rho_{\alpha\beta}(t) = -i(\epsilon_\alpha - \epsilon_\beta)\rho_{\alpha\beta}(t) + \sum_{\alpha'\beta'} L_{\alpha\beta\alpha'\beta'}(t)\rho_{\alpha'\beta'}(t), \tag{B2}$$

where $\rho_{\alpha\beta}(t) = \langle u_\alpha(t)|\,\rho(t)\,|u_\beta(t)\rangle$ are the components of the system's density matrix in a Floquet basis. The first term in Eq. (B2) corresponds to the unitary evolution of the system, while the second one takes into account dissipative effects. The transition rates $L_{\alpha\beta\alpha'\beta'}(t)$ are T periodic and can be Fourier-expanded as

$$L_{\alpha\beta\alpha'\beta'}(t) = \sum_q L^q_{\alpha\beta\alpha'\beta'} e^{-iq\omega t}, \tag{B3}$$

with $q \in \mathbb{Z}$, and where the coefficients $L^q_{\alpha\beta\alpha'\beta'}$ are given by

$$L^q_{\alpha\beta\alpha'\beta'} = \lambda^2 \sum_k \Big[g^k_{\alpha\alpha'} A^k_{\alpha\alpha'} A^{-k-q}_{\beta'\beta} + g^k_{\beta\beta'} A^{k-q}_{\alpha\alpha'} A^{-k}_{\beta'\beta} - \sum_\eta \left(\delta_{\beta\beta'} g^k_{\eta\alpha'} A^{-k-q}_{\alpha\eta} A^k_{\eta\alpha'} + \delta_{\alpha\alpha'} g^k_{\eta\beta'} A^{-k}_{\beta'\eta} A^{k-q}_{\eta\beta} \right) \Big]. \tag{B4}$$

In the last expression, the index η runs over the indices of the Floquet basis, $\delta_{\alpha\beta}$ is the Kronecker delta, and we define

$$A^q_{\alpha\beta} = \sum_k \left\langle u^k_\alpha \middle| A \middle| u^{q+k}_\beta \right\rangle \tag{B5}$$

and

$$g^k_{\alpha\beta} = g(\epsilon_\alpha - \epsilon_\beta + k\omega). \tag{B6}$$

In Eq .(B5), $|u^k_\alpha\rangle$ is the kth Fourier component of the Floquet state $|u_\alpha(t)\rangle$. In Eq. (B6), $g(\omega')$ is the Fourier-transformed correlation function of the thermal bath, which can be expressed in terms of its spectral density and the Bose occupation number $n_{T_{\mathrm{b}}}(\omega') = 1/(e^{\omega'/T_{\mathrm{b}}} - 1)$ as

$$g(\omega') = \begin{cases} \mathcal{J}(\omega') n_{T_{\mathrm{b}}}(\omega') & \Leftarrow \omega' > 0, \\ -\mathcal{J}(-\omega') n_{T_{\mathrm{b}}}(\omega') & \Leftarrow \omega' < 0, \end{cases} \tag{B7}$$

with the value of g at $\omega' = 0$ obtained by taking the appropriate limit.

For sufficiently weak coupling to the environment, such that the maximum rate of relaxation or decoherence is much smaller than the driving frequency, a (moderate) RWA is justified in the transition rates, Eq. (B3). This sets the terms with $q \neq 0$ effectively to zero, yielding the simplified expression

$$L_{\alpha\beta\alpha'\beta'} \approx R_{\alpha\beta\alpha'\beta\beta'} + R^*_{\beta\alpha\beta'\alpha'} - \sum_\eta (\delta_{\beta\beta'} R_{\eta\eta\alpha'\alpha} + \delta_{\alpha\alpha'} R^*_{\eta\eta\beta'\beta}), \tag{B8}$$

in terms of the quantities

$$R_{\alpha\beta\alpha'\beta'} = \sum_k g^k_{\alpha\alpha'} A^k_{\alpha\alpha'} A^{-k}_{\beta\beta'}. \tag{B9}$$

With this approximation, Eq. (B2) no longer depends explicitly on time in the Floquet basis.

For the cases studied in this work, it was found that the operator $\Lambda_{\alpha\beta\alpha'\beta'} = -i(\epsilon_\alpha - \epsilon_\beta)\delta_{\alpha\alpha'}\delta_{\beta\beta'} + L_{\alpha\beta\alpha'\beta'}$ can be numerically diagonalized in terms of left and right eigenvectors

which are density matrices. That is,

$$\Lambda\rho_\mu^{\mathrm{R}} = \rho_\mu^{\mathrm{L}}\Lambda = \zeta_\mu\rho_\mu, \tag{B10}$$

with $\zeta_\mu \in \mathbb{C}$ and $\frac{1}{N}\mathrm{Tr}(\rho_\mu^{\mathrm{L}}\rho_\nu^{\mathrm{R}}) = \delta_{\mu\nu}$, where N is the dimension of the system's Hilbert space. Once these eigenvectors and eigenvalues are obtained, density matrices can be evolved readily by projecting on this eigensystem

$$\rho(t) = \sum_\mu c_\mu e^{\zeta_\mu(t-t_0)}\rho_\mu^{\mathrm{R}}, \quad c_\mu = \frac{1}{N}\mathrm{Tr}[\rho_\mu^{\mathrm{L}}\rho(t_0)]. \tag{B11}$$

The real parts of ζ_μ (which are always negative) are the decoherence and relaxation rates. In particular, the maximum relaxation rate can be defined as

$$\gamma_M \equiv \max_\mu|\mathrm{Re}(\zeta_\mu)|. \tag{B12}$$

The regime of validity of the Floquet-Born-Markov equation [57,58] in terms of γ_M turns out to be

$$\gamma_M < T_{\mathrm{b}}. \tag{B13}$$

For every open system simulation performed in this work we calculated numerically the relaxation rate γ_M and checked the validity of the condition of Eq. (B13).

The stationary state ρ_∞, which for all cases studied in this work can be found and is unique, is defined (in the Floquet basis) as the state ρ_μ^{R} with $\zeta_\mu = 0$. It is constant in the Floquet basis and therefore T periodic in the original system basis.

The numerical procedure used here to solve the Floquet-Born-Markov equation and to obtain $\rho(t)$ and ρ_∞ was described in Ref. [41]. To calculate time-averaged functions $f(\rho)$ of the system's density matrix in the stationary state, such as populations or concurrence, we make use of the periodicity of ρ_∞ and numerically integrate

$$\bar{f} = \frac{1}{T}\int_0^T dt\, f[\rho_\infty(t)]. \tag{B14}$$

APPENDIX C: $N\pm$ AVOIDED CROSSINGS AND ASSOCIATED PARENT HAMILTONIAN

In this section we will derive a Hamiltonian that describes well the $N\pm$ AC located at $\epsilon = \pm\Omega$ (see Fig. 2). For concreteness we will focus on the AC $N+$ at $\epsilon = +\Omega$ and the treatment for the $\epsilon = -\Omega$ case is similar. Starting from the Hamiltonian of Eq. (3), we can rewrite the interaction term between the qubits and the resonator in terms of the qubit ladder operators $\sigma_\pm^{(i)} = \frac{1}{2}(\sigma_x^{(i)} \pm i\sigma_y^{(i)})$, obtaining

$$H = \Omega a^\dagger a + \sum_i \Big(\frac{\epsilon}{2}\sigma_z^{(i)} + g_i a\sigma_+^{(i)} + g_i a\sigma_-^{(i)} + g_i a^\dagger\sigma_+^{(i)} + g_i a^\dagger\sigma_-^{(i)}\Big). \tag{C1}$$

Assuming $|\epsilon - \Omega| \ll \Omega$, the terms proportional to $\sigma_+^{(i)}a$ and $\sigma_-^{(i)}a^\dagger$ approximately conserve the energy of the uncoupled system, while the terms proportional to $\sigma_+^{(i)}a^\dagger$ and $\sigma_-^{(i)}a$ do not. For small coupling strengths $g_i \ll \Omega$ it is customary to apply a RWA in which the terms that do not conserve the energy of the uncoupled system are set to zero.

With this approximation applied, the Hamiltonian Eq. (C1) becomes block diagonal, where each block has a fixed total excitation number $N' = a^\dagger a + n_1 + n_2$, where $n_i = \frac{1}{2}(1 + \sigma_z^{(i)})$ is the qubit i excitation number. Notice that $N' = N + 1$, with N corresponding to the integer associated to the $N\pm$ AC. Restricting ourselves to the block with N' total excitations, we can write

$$\begin{aligned} a^\dagger a &= N' - n_1 - n_2 \\ &= N' - \frac{1}{2}\big(1 + \sigma_z^{(1)}\big) - \frac{1}{2}\big(1 + \sigma_z^{(2)}\big) \\ &= -\frac{\sigma_z^{(1)} + \sigma_z^{(2)}}{2} + N' - 1, \end{aligned} \tag{C2}$$

and

$$(a + a^\dagger)\sigma_x^{(1)} \overset{\mathrm{RWA}}{\approx} \sigma_+^{(1)}a + \sigma_-^{(1)}a^\dagger = \sqrt{N' - n_2}\,\sigma_x^{(1)}, \tag{C3}$$

for the coupling term between the qubit 1 and the resonator. Now we use that n_2 can take only the values 0 and 1 and write

$$\begin{aligned} &(a + a^\dagger)\sigma_x^{(1)} \\ &\overset{\mathrm{RWA}}{\approx} ((1 - n_2)\sqrt{N'} + n_2\sqrt{N' - 1})\sigma_x^{(1)} \\ &= \frac{1}{2}\Big(\big(1 - \sigma_z^{(2)}\big)\sqrt{N'} + \big(1 + \sigma_z^{(2)}\big)\sqrt{N' - 1}\Big)\sigma_x^{(1)} \\ &= \frac{\sqrt{N'} + \sqrt{N' - 1}}{2}\sigma_x^{(1)} - \frac{\sqrt{N'} - \sqrt{N' - 1}}{2}\sigma_x^{(1)}\sigma_z^{(2)}, \\ &= \sqrt{N'}_+\sigma_x^{(1)} - \sqrt{N'}_-\sigma_x^{(1)}\sigma_z^{(2)}. \end{aligned} \tag{C4}$$

where we define $\sqrt{N'}_\pm = \frac{1}{2}(\sqrt{N'} \pm \sqrt{N' - 1})$. Performing the same procedure for the qubit 2 and then replacing Eqs. (C2) and (C4) in Eq. (C1), we arrive at an effective Hamiltonian for the block with $N' \geqslant 1$ excitations

$$\begin{aligned} H_{N'} = &\sum_{i=1}^{2}\Big(\frac{\epsilon - \Omega}{2}\sigma_z^{(i)} + g_i\sqrt{N'}_+\sigma_x^{(i)}\Big) \\ &- \sqrt{N'}_-(g_1\sigma_x^{(1)}\sigma_z^{(2)} + g_2\sigma_z^{(1)}\sigma_x^{(2)}) + (N' - 1)\Omega \end{aligned} \tag{C5}$$

that can be cast in terms of $g \equiv (g_1 + g_2)/2$ and δ_g as

$$\begin{aligned} H_{N'} = &\frac{\epsilon - \Omega}{2}\sum\sigma_z^i \\ &+ g\big(\sqrt{N'}_+\big(\sigma_x^1 + \sigma_x^2\big) - \sqrt{N'}_-\big(\sigma_x^1\sigma_z^2 + \sigma_z^1\sigma_x^2\big)\big) \\ &+ \frac{\delta_g}{2}\big(\sqrt{N'}_+\big(\sigma_x^1 - \sigma_x^2\big) - \sqrt{N'}_-\big(\sigma_x^1\sigma_z^2 - \sigma_z^1\sigma_x^2\big)\big). \end{aligned} \tag{C6}$$

In the above equation, the operator multiplied by g has $|N\Psi_-\rangle$ as an eigenstate with zero eigenvalue as can be readily verified, and therefore will only generate transitions between the states $|(N \mp 1)\uparrow\uparrow\rangle$, $|N\Psi_+\rangle$, and $|(N \pm 1)\downarrow\downarrow\rangle$. For $N' > 1$, the dominant term in this operator goes as $\sqrt{N'}g = \sqrt{N + 1}g$. On the other hand, the operator proportional to δ_g induces transitions between $|N\Psi_-\rangle$ and the other states, with a magnitude that goes for $N' > 1$ approximately as $\sqrt{N'}\delta_g = \sqrt{N + 1}\delta_g$. When $\epsilon \approx \Omega$, these terms will dominate in the Hamiltonian $H_{N'}$, generating AC with energy gaps of the aforementioned magnitudes. After including driving, the LZS transitions will be ruled by these AC.

Moreover, the term proportional to g in Eq. (C6) is controlled by the $(\sigma_x^1 + \sigma_x^2)$ operator for $N' > 1$. This operator, when acted on $|(N \mp 1)\uparrow\uparrow\rangle$ or $|(N \pm 1)\downarrow\downarrow\rangle$, yields a state proportional to $|N\Psi_+\rangle$. This means that in these AC the state $|(N \pm 1)\downarrow\downarrow\rangle$ is mixed with $|N\Psi_+\rangle$ more strongly than with $|(N \mp 1)\uparrow\uparrow\rangle$, and similarly for the $|(N \mp 1)\uparrow\uparrow\rangle$ state. This justifies neglecting the transitions between $|(N \mp 1)\uparrow\uparrow\rangle$ and $|(N \pm 1)\downarrow\downarrow\rangle$ in the $N\pm$ AC to obtain the effective Hamiltonians derived in Sec. III.

[1] B. Kraus, H. P. Büchler, S. Diehl, A. Kantian, A. Micheli, and P. Zoller, Phys. Rev. A **78**, 042307 (2008).

[2] F. Verstraete, M. M. Wolf, and J. Ignacio Cirac, Nat. Phys. **5**, 633 (2009).

[3] F. Tacchino, A. Auffèves, M. F. Santos, and D. Gerace, Phys. Rev. Lett. **120**, 063604 (2018).

[4] P. Král, I. Thanopulos, and M. Shapiro, Rev. Mod. Phys. **79**, 53 (2007).

[5] H. Maeda, J. H. Gurian, D. V. L. Norum, and T. F. Gallagher, Phys. Rev. Lett. **96**, 073002 (2006).

[6] B. B. Zhou, A. Baksic, H. Ribeiro, C. Yale, F. Heremans, P. Jerger, A. Auer, G. Burkard, A. Clerk, and D. Awschalom, Nat. Phys. **13**, 330 (2017).

[7] S. Shankar, M. Hatridge, Z. Leghtas, K. Sliwa, A. Narla, U. Vool, S. M. Girvin, L. Frunzio, M. Mirrahimi, and M. H. Devoret, Nature (London) **504**, 419 (2013).

[8] Z. Leghtas, U. Vool, S. Shankar, M. Hatridge, S. M. Girvin, M. H. Devoret, and M. Mirrahimi, Phys. Rev. A **88**, 023849 (2013).

[9] M. E. Kimchi-Schwartz, L. Martin, E. Flurin, C. Aron, M. Kulkarni, H. E. Tureci, and I. Siddiqi, Phys. Rev. Lett. **116**, 240503 (2016).

[10] C. M. Quintana, K. D. Petersson, L. W. McFaul, S. J. Srinivasan, A. A. Houck, and J. R. Petta, Phys. Rev. Lett. **110**, 173603 (2013).

[11] P. Campagne-Ibarcq, E. Zalys-Geller, A. Narla, S. Shankar, P. Reinhold, L. Burkhart, C. Axline, W. Pfaff, L. Frunzio, R. J. Schoelkopf, and M. H. Devoret, Phys. Rev. Lett. **120**, 200501 (2018).

[12] R. Li, D. Yu, S.-L. Su, and J. Qian, Phys. Rev. A **101**, 042328 (2020).

[13] H. Krauter, C. A. Muschik, K. Jensen, W. Wasilewski, J. M. Petersen, J. I. Cirac, and E. S. Polzik, Phys. Rev. Lett. **107**, 080503 (2011).

[14] J. T. Barreiro, M. Müller, P. Schindler, D. Nigg, T. Monz, M. Chwalla, M. Hennrich, C. F. Roos, P. Zoller, and R. Blatt, Nature (London) **470**, 486 (2011).

[15] Y. Lin, J. P. Gaebler, F. Reiter, T. R. Tan, R. Bowler, A. S. Sørensen, D. Leibfried, and D. J. Wineland, Nature **504**, 415 (2013).

[16] D. Kienzler, H.-Y. Lo, B. Keitch, L. de Clercq, F. Leupold, F. Lindenfelser, M. Marinelli, V. Negnevitsky, and J. P. Home, Science **347**, 53 (2015).

[17] L. DiCarlo, M. D. Reed, L. Sun, B. R. Johnson, J. M. Chow, J. M. Gambetta, L. Frunzio, S. M. Girvin, M. H. Devoret, and R. J. Schoelkopf, Nature (London) **467**, 574 (2010).

[18] A. L. Gramajo, D. Domínguez, and M. J. Sánchez, Phys. Rev. A **98**, 042337 (2018).

[19] A. L. Gramajo, D. Domínguez, and M. J. Sánchez, Phys. Rev. A **104**, 032410 (2021).

[20] A. Blais, R.-S. Huang, A. Wallraff, S. M. Girvin, and R. J. Schoelkopf, Phys. Rev. A **69**, 062320 (2004).

[21] A. Wallraff, D. I. Schuster, A. Blais, L. Frunzio, R.-S. Huang, J. Majer, S. Kumar, S. M. Girvin, and R. J. Schoelkopf, Nature (London) **431**, 162 (2004).

[22] Z.-L. Xiang, S. Ashhab, J. Q. You, and F. Nori, Rev. Mod. Phys. **85**, 623 (2013).

[23] A. Blais, S. M. Girvin, and W. D. Oliver, Nat. Phys. **16**, 247 (2020).

[24] A. Blais, A. L. Grimsmo, S. M. Girvin, and A. Wallraff, Rev. Mod. Phys. **93**, 025005 (2021).

[25] J. Koch, T. M. Yu, J. Gambetta, A. A. Houck, D. I. Schuster, J. Majer, A. Blais, M. H. Devoret, S. M. Girvin, and R. J. Schoelkopf, Phys. Rev. A **76**, 042319 (2007).

[26] X. Gu, A. F. Kockum, A. Miranowicz, Y. Liu, and F. Nori, Phys. Rep. **718–719**, 1 (2017).

[27] M. Bonifacio, D. Domínguez, and M. J. Sánchez, Phys. Rev. B **101**, 245415 (2020).

[28] J. M. Fink, R. Bianchetti, M. Baur, M. Göppl, L. Steffen, S. Filipp, P. J. Leek, A. Blais, and A. Wallraff, Phys. Rev. Lett. **103**, 083601 (2009).

[29] H. Paik, D. I. Schuster, L. S. Bishop, G. Kirchmair, G. Catelani, A. P. Sears, B. R. Johnson, M. J. Reagor, L. Frunzio, L. I. Glazman, S. M. Girvin, M. H. Devoret, and R. J. Schoelkopf, Phys. Rev. Lett. **107**, 240501 (2011).

[30] A. Dewes, R. Lauro, F. R. Ong, V. Schmitt, P. Milman, P. Bertet, D. Vion, and D. Esteve, Phys. Rev. B **85**, 140503(R) (2012).

[31] L. DiCarlo, J. M. Chow, J. M. Gambetta, L. S. Bishop, B. R. Johnson, D. Schuster, J. Majer, A. Blais, L. Frunzio, S. Girvin *et al.*, Nature (London) **460**, 240 (2009).

[32] M. Stern, G. Catelani, Y. Kubo, C. Grezes, A. Bienfait, D. Vion, D. Esteve, and P. Bertet, Phys. Rev. Lett. **113**, 123601 (2014).

[33] B. R. Johnson, M. D. Reed, A. A. Houck, D. I. Schuster, L. S. Bishop, E. Ginossar, J. M. Gambetta, L. DiCarlo, L. Frunzio, S. M. Girvin, and R. J. Schoelkopf, Nat. Phys. **6**, 663 (2010).

[34] T. Walter, P. Kurpiers, S. Gasparinetti, P. Magnard, A. Potočnik, Y. Salathé, M. Pechal, M. Mondal, M. Oppliger, C. Eichler, and A. Wallraff, Phys. Rev. Applied **7**, 054020 (2017).

[35] A. F. van Loo, A. Fedorov, K. Lalumiere, B. C. Sanders, A. Blais, and A. Wallraff, Science **342**, 1494 (2013).

[36] C. Eichler, C. Lang, J. M. Fink, J. Govenius, S. Filipp, and A. Wallraff, Phys. Rev. Lett. **109**, 240501 (2012).

[37] N. Didier, J. Bourassa, and A. Blais, Phys. Rev. Lett. **115**, 203601 (2015).

[38] S. N. Shevchenko, S. Ashhab, and F. Nori, Phys. Rep. **492**, 1 (2010).

[39] W. D. Oliver and S. O. Valenzuela, Quant. Info. Proc. **8**, 261 (2009).

[40] A. Ferrón, D. Domínguez, and M. J. Sánchez, Phys. Rev. Lett. **109**, 237005 (2012).

[41] A. Ferrón, D. Domínguez, and M. J. Sánchez, Phys. Rev. B **93**, 064521 (2016).

[42] A. L. Gramajo, D. Domínguez, and M. J. Sánchez, Phys. Rev. B **100**, 075410 (2019).

[43] N. T. Bronn, E. Magesan, N. A. Masluk, J. M. Chow, J. M. Gambetta, and M. Steffen, IEEE Trans. Appl. Supercond. **25**, 1 (2015).
[44] W. D. Oliver, Y. Yu, J. C. Lee, K. K. Berggren, L. S. Levitov, and T. P. Orlando, Science **310**, 1653 (2005).
[45] J. H. Shirley, Phys. Rev. **138**, B979 (1965).
[46] S. Kohler, R. Utermann, P. Hänggi, and T. Dittrich, Phys. Rev. E **58**, 7219 (1998).
[47] R. Blattmann, P. Hänggi, and S. Kohler, Phys. Rev. A **91**, 042109 (2015).
[48] S. Ashhab, J. R. Johansson, A. M. Zagoskin, and F. Nori, Phys. Rev. A **75**, 063414 (2007).
[49] A. Ferrón and D. Domínguez, Phys. Rev. B **81**, 104505 (2010).
[50] F. Forster, G. Petersen, S. Manus, P. Hänggi, D. Schuh, W. Wegscheider, S. Kohler, and S. Ludwig, Phys. Rev. Lett. **112**, 116803 (2014).
[51] J. V. Koski, A. J. Landig, A. Pályi, P. Scarlino, C. Reichl, W. Wegscheider, G. Burkard, A. Wallraff, K. Ensslin, and T. Ihn, Phys. Rev. Lett. **121**, 043603 (2018).
[52] A. L. Gramajo, D. Campbell, B. Kannan, D. K. Kim, A. Melville, B. M. Niedzielski, J. L. Yoder, M. J. Sánchez, D. Domínguez, S. Gustavsson, and W. D. Oliver, Phys. Rev. Applied **14**, 014047 (2020).
[53] M. Grifoni and P. Hänggi, Phys. Rep. **304**, 229 (1998).
[54] A. L. Gramajo, D. Domínguez, and M. J. Sánchez, Eur. Phys. J. B **90**, 255 (2017).
[55] W. K. Wootters, Phys. Rev. Lett. **80**, 2245 (1998).
[56] H.-P. Breuer and F. Petruccione, *The Theory of Open Quantum Systems* (Oxford University Press, Oxford, 2006).
[57] S. Kohler, T. Dittrich, and P. Hänggi, Phys. Rev. E **55**, 300 (1997).
[58] D. W. Hone, R. Ketzmerick, and W. Kohn, Phys. Rev. E **79**, 051129 (2009).